J. Phys. B: At. Mol. Phys. **17** (1984) 1137–1154. Printed in Great Britain

Resonant electron attachment to oxygen molecules in dense helium gas†

L Bruschi, M Santini and G Torzo

Dipartimento di Fisica dell'Università di Padova and Gruppo Nazionale Struttura della Materia, Padova, Italy

Received 8 July 1983, in final form 3 November 1983

Abstract. Measurements of the resonant attachment frequency of excess electrons to O_2 molecules in dense helium gas have been performed in the temperature range 50–100 K. The attachment frequency exhibits a sharp peak at a density N_P, which has an unexpected temperature dependence. The peak shape has been simply related to the density dependence of $F(E_R)$, the value of the energy distribution function at the resonance energy E_R. The results of the experiment indicate that resonant capture by molecular impurities can be used to get unique information on the density of states of a disordered system.

1. Introduction

The electron attachment to oxygen molecules is a well studied phenomenon (Herzenberg 1969, Christophorou 1971, Hatano and Shimamori 1981). It can be described by the so-called Bloch–Bradbury two-stage process

$$\begin{aligned} &e^- + O_2 \rightarrow O_2^{-*} \\ &O_2^{-*} + B \rightarrow O_2^- + B \end{aligned} \tag{1}$$

where O_2^{-*} is an unstable negative ion in a vibrationally excited state (Boness *et al* 1970), and B is a third body that carries out the excess energy in a stabilising collision. In our case the oxygen molecules are present at very low concentrations, so that B may be assumed to always be a helium atom. The colliding electron energy must be exactly equal to the difference E_n between the energy of an excited ion state O_2^{-*} and that of the neutral oxygen molecule ground state. The energy E_n for the first accessible level is $E_4 = 0.091$ eV.

The first experimental evidence of resonant attachment to O_2 molecules in high-density helium gas is due to Bartels (1973). He worked at 77 K and he found a sharp maximum of the attachment frequency ν_A at a density $N \simeq 30 \times 10^{20}\,\mathrm{cm}^{-3}$. In this type of experiment the thermal energy is only a minor contribution to the resonance energy, because $k_B T \ll E_4$. The most important contribution is due to the Fermi shift

$$E_0 = (2\pi\hbar^2/m)\, aN \tag{2}$$

where m is the electron mass, a is the electron–helium scattering length and N is the helium number density (Fermi 1934, Burdick 1965, Jortner *et al* 1965). The maximum in the attachment frequency occurs at a density N_4 where $E_0(N_4) \simeq E_4$.

† Work sponsored by Consiglio Nazionale delle Ricerche and Ministero Pubblica Istruzione, Roma, Italy.

Using different molecular impurities, different attachment peaks could be detected. If a relationship between the resonant density and the Fermi shift E_0 is available, then E_0 can be measured as a function of the number density N. The energy E_0 has been measured by various authors, as an energy barrier for electron injection into liquid from free surface (Sommer 1964), by photoinjection or field emission from metallic electrode (Woolf and Rayfield 1965, Tauchert *et al* 1977), photoinjection from pseudobubbles (Northby and Sanders 1967), and tunnelling escape from electronic surface states (Schoepe and Rayfield 1973). The value of E_0 is not derived directly in these experiments but it is obtained through calculations that require a detailed knowledge of the fluid electrode interface, of the liquid free surface, and of the pseudobubble structure. All these experiments involve surface effects not easy to handle, and the agreement between experiments and between experiments and theory is not good. It is therefore interesting to try a different method that allows bulk measurements of E_0 avoiding any surface effect. Moreover the shape of the resonance peak can yield useful information on the density of electronic states. In fact the attachment occurs only for electrons whose energy is equal to the resonant energy E_R. The attachment frequency ν_A is therefore proportional to the value of the energy distribution function $F(E_R, N)$ at $E = E_R$. The peak gives direct information on the density dependence of the energy distribution function near the resonant energy, and its measurement can be a good test of the theories of electronic states of disordered systems.

2. Experimental

2.1. The method of measurement

Let us refer to figure 1(*a*). S′ and C are two plane and parallel electrodes, a distance d apart, immersed in the fluid to be studied. S′ is an emitter that injects thermalised electrons at $x = 0$, and it is kept at a negative potential $(-V_0)$ with respect to the collector C; suppose now that a thin slice of such electrons is injected at time $t = 0$, with a number density $n(0)$. It drifts towards the collector with drift velocity v_D, and because electrons suffer attaching collisions with the oxygen impurities, the electron density decreases according to the exponential law

$$n(t) = n(0) \exp(-t/\tau) = n(0) \exp(-t\nu_A) \tag{3}$$

where τ is the mean life of the electrons, and $\nu_A = (1/\tau)$ is the attachment frequency. When electrons reach a distance $x = v_D t$ from the emitter, their density will be

$$n(x) = n(0) \exp(-x/\lambda) \tag{4}$$

where $\lambda = (v_D/\nu_A)$ is the attenuation coefficient.

If the injection is continuous, as in our experiments, and the electric field is uniform over the whole measuring space, the electronic currents I_e and I_0 at the collector and at the emitter are related by the relation

$$(I_e/I_0) = n(d)/n(0) = \exp(-d/\lambda). \tag{5}$$

From a measurement of the ratio (I_e/I_0) we get $(1/\lambda) = \ln(I_0/I_e)/d$. If we also measure the drift velocity v_D we get the attachment rate

$$\nu_A = (v_D/\lambda) = (v_D/d) \ln(I_0/I_e). \tag{6}$$

This is essentially the principle of the method.

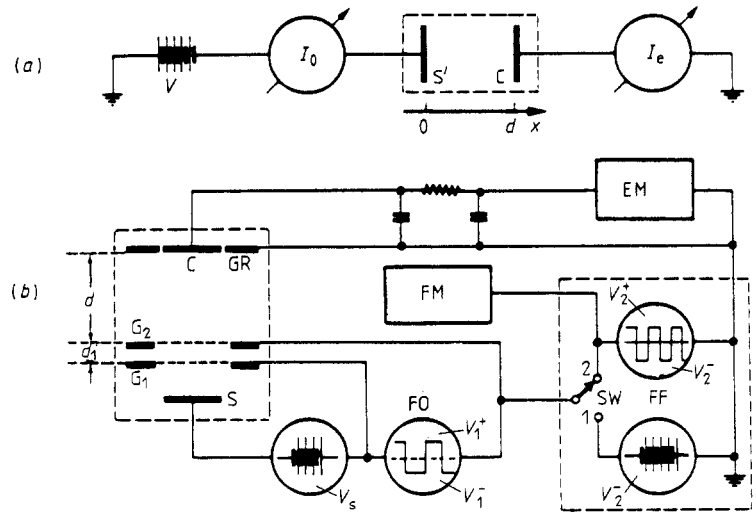

Figure 1. Schematic diagram of the measuring apparatus. (*a*) Simplified picture. (*b*) Actual arrangement. The ideal electron emitter S' is obtained by means of the radioactive source S and the grids G_1 and G_2. G_2 is driven by the presettable unbalanced flip-flop FF, and G_1 is driven by FF through the floating unbalanced square-wave generator FO. GR is the guard ring, EM the electrometer and FM the frequency meter.

The injected current I_0 must be a pure electronic current. We need, therefore, an emitter that injects only electrons, rejecting ions that may be present at $x=0$. At the collector the current is the sum of an electronic part I_e and an ionic one I_i, with $I_0 = I_e + I_i$. The measurement of I_e while rejecting I_i can be done using AC techniques, because the electronic and ionic mobilities are very different, $(\mu_i/\mu_e) \simeq 10^{-3}$.

The above requirements can be satisfied by our technique, that is a modified version of the well known square-wave method (Cunsolo 1961). The electrode set-up is shown in figure 1(*b*). A radioactive source ionises a fluid layer near the emitter S, which is kept at a negative potential with respect to the grid G_1. Electrons drift from S towards G_1, and because of the attachment process both electrons and ions reach G_1. This grid is driven, with respect to G_2, by a square-wave signal V_1 of frequency $f_1 = (2T_1)^{-1}$. Because electronic and ionic mobilities are so different, the half period T_1 can be chosen to be much shorter than the ionic transit time across G_1G_2, but still longer than the electronic one. Therefore the ions generated behind G_1 and passing through it, cannot reach G_2 during the injecting half period ($V_1 < 0$). They are later cleaned out from the G_1G_2 space and collected at G_1 in the following half period ($V_1 > 0$). Electrons, however, can pass through G_2, and G_2 acts as a very effective electron injector. Only the ions born very close to G_2 can pass through during the injecting half period, and by a proper choice of T_1, the ionic current through G_2 can be reduced to a negligible level (Bruschi *et al* 1983). Most of the ions produced between G_1 and G_2 cannot ever reach G_1 or G_2. They keep on oscillating between the two grids and pile-up occurs. To avoid their injection into the drift space by space charge or by diffusion, we used an unbalanced square wave ($V_1^+ > V_1^-$). In this way the ions produced across G_1G_2 go to and fro, but on average they move back to G_1. The pile-up of negative ions across G_1 and G_2 is avoided, and the grid acts as a pulsed pure electronic source.

Now let the grid G_2 be driven, with respect to the collector C, by a square wave V_2 of frequency $f = (2T)^{-1}$. Suppose for the moment that only electrons are present

in the drift space G_2C. If τ_e is the electron transit time across G_2C, then the mean current measured at the collector is given by

$$\begin{aligned} &\bar{i}=0 && \text{for } f>f_e \\ &\bar{i}=(I_0/2)(1-f/f_e) && \text{for } f\leqslant f_e \end{aligned} \tag{7}$$

where $f_e=(2\tau_e)^{-1}$, and I_0 is the injected current at G_2 (Cunsolo 1961).

The situation of interest is more complicated, because both electrons and ions are present in the drift space. Let us consider two frequency regions: $f\leqslant f_i$, and $f\geqslant f_i$, where f_i is the ion cut-off frequency, $f_i=(2\tau_i)^{-1}$, and τ_i is the ionic transit time. When $f<f_i$ the ions generated near G_2 also have enough time to reach the collector, and $\bar{i}$ is the sum of the contributions of both electronic and ionic currents. It is easy to see that the mean current $\bar{i}$ in this frequency region is linearly dependent on f, and for $f\to 0$, $\bar{i}(0)=(I_0/2)$. This low-frequency region is not particularly interesting for our purposes.

For $f\geqslant f_i$ the dependence is not very simple. For $f\gg f_i$, however, only ions created very near the collector can reach it, so that ionic current is negligible, and $\bar{i}$ is again linear to a very good approximation

$$\begin{aligned} &\bar{i}=0 && \text{for } f>f_e \\ &\bar{i}=I^*(1-f/f_e) && \text{for } f_i\ll f\leqslant f_e. \end{aligned} \tag{8}$$

The linear relation (8) is valid only in the indicated frequency region. If the current measured in this region is extrapolated back to $f\to 0$, one obtains the value I^*. This is essentially the contibution, at $f=0$, given by the electronic current to the total collector current. If only fast electrons are present, it must be $I^*=(I_0/2)$. If the attachment process is effective, not all the injected electrons reach the collector, and I^* should be attenuated according to relation (5)

$$I^*=(I_0/2)\exp(-d/\lambda). \tag{9}$$

Now $\nu_A=(v_D/\lambda)=(d/\tau_e\lambda)=2f_e(d/\lambda)$, and from (9) we have finally

$$\nu_A=2f_e\ln(I_0/2I^*) \tag{10}$$

while the electronic mobility μ_e is given by

$$\mu_e=2d^2f_e/V_2 \tag{11}$$

where V_2 is the amplitude of the square-wave voltage applied to G_2.

A sketch of the whole dependence of $\bar{i}$ on f, for $(d/\lambda)=1$ and $(\mu_e/\mu_i)=100$ is reported in figure 2. The above results are essentially confirmed by a more complete analysis (Bruschi *et al* 1983), which yields

$$\begin{aligned} &\bar{i}=0 && \text{for } f>f_e \\ &\bar{i}=I^*(1-f/f_e)G(z) && \text{for } f_i<f<f_e \end{aligned} \tag{12}$$

where $G(z)=[\exp(z)-1]/z$, and $z=\frac{1}{2}(1-f/f_e)\nu_A\mu_i/(\mu_e-\mu_i)$. For small z, $G(z)\simeq 1$ and (12) reduces to (8). If one wants the correcting factor $G(z)$ to be smaller than $(1+\varepsilon)$, one must work at frequencies

$$f>f_e\left[1+\frac{4f_e}{\nu_A}\left(\frac{\mu_e}{\mu_i}-1\right)\varepsilon\right]^{-1}. \tag{13}$$

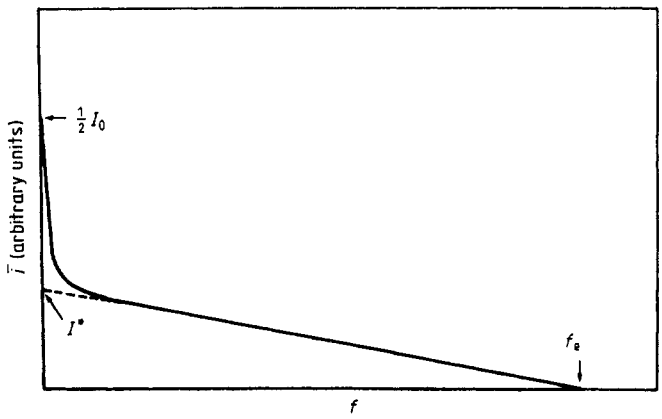

Figure 2. Behaviour of the collected current $\bar{I}$ plotted against frequency f, as given by relation (12), for $d/\lambda = 1$ and $\mu_e/\mu_i = 100$.

Relation (13) can be used to choose the frequency range appropriate to the requested accuracy. The problem of molecular ions created and trapped in the drift space is the same as that previously examined for the G_1G_2 region, and it is solved in the same way. The amplitude V_2^+ of the positive part of the square-wave voltage V_2 is made greater than the negative one ($V_2^+ > V_2^-$). In this way the ions oscillate, but on the average they move back to G_2, and the pile-up of negative charge is avoided.

2.2. Experimental details

The measuring cell is made of brass and it can work at pressures up to 70 atm. The grids G_1, G_2, the collector C and the guard ring GR are conventional gold-plated electrodes, separated by plexiglass spacers. The source is a β emitter, made by ^{63}Ni electroplated on nickel, with an activity of 5 mCi (Radiochemical Centre, Amersham). This source was preferred to other sources (^{241}Am in gold matrix, ^{3}H absorbed in titanium) because it is practically free from bremsstrahlung γ rays, while the moderate β energy (66 keV) offers a rather short ionisation range.

A constant negative potential V_s(10–30 V) is applied to S with respect to G_1, so that only negative charges are extracted from the ionisation space. V_s is generated by a floating battery.

The grid G_1 is driven by a floating unbalanced square-wave generator (FO), (0–100 V), that is specially designed to have a small capacity with respect to ground (Bruschi *et al* 1983).

The grid G_2 is driven by a home made presettable unbalanced flip-flop (FF) that can work with a maximum swing of 270 V and a rise time $t_r < 1\ \mu s$. A pair of conventional low-noise high-stability power supplies accomplishes the separate adjustment of V_2^+ and V_2^-. To measure the total current I_0 (FF) is blocked on the pre-set state $V_{out} = V_2^-$.

The collected current is integrated and measured by a Keithley 640 vibrating capacitor picoammeter (EM). Typical values of the current I_0 injected in the drift space were 10^{-12}–10^{-10} A, while the extrapolated value I^* was obviously a function of the attachment efficiency.

The cell was usually submerged in a liquid nitrogen bath. A 77 K radiator shield is provided by an outer liquid nitrogen bath. Temperatures lower than the normal

boiling point were simply reached by pumping on the bath. When temperatures higher than the normal boiling point were wanted, the liquid nitrogen level was kept below the cell bottom. Stabilisation, to within 10^{-2} K, is achieved by a thermoregulator that drives a heater wound around the cell. The temperature is measured by means of a calibrated platinum thermometer (Rosemount 118 MF), placed inside the cell. The pressure of the sample fluid is measured to within 10^{-2} atm by an Ashcroft Digigauge model 7780, and the fluid number density N is calculated from the virial equation using the Leiden coefficients (Cook 1961). The He sample gas has a nominal purity of 99.9996% and a nominal oxygen content of less than 2 ppm. It was slowly fed to the cell through an active charcoal trap cooled by liquid nitrogen. A good clean-up performance was obtained using two elements in series, filled with compressed thin charcoal powder after a very long degassing at high temperature.

3. Experimental results

3.1. Oxygen concentration

As stated in the introduction the attachment rate depends on helium number density. Moreover it must depend linearly on the oxygen number density. At constant pressure and temperature, ν_A must therefore be simply proportional to the oxygen concentration C. To verify that our method of measurement works correctly, we performed a check of the dependence of ν_A on the concentration C. We mixed at room temperature oxygen at some low pressure P_1 with 'pure' He at some high pressure P_2. We pumped out the mixture down to P_1, and refilled up to P_2 with new 'pure' He, and so on. After some steps we obtained a mixture with a known concentration C_0 (typical value $C_0 = 10^{-5}$). At this point the mixture was transferred into the measuring cell, and diluted again with the same procedure using partially purified helium with an unknown low concentration C_P. We diluted the mixture lowering the nominal concentration by a factor of two each step. ($P_2/P_1 = 2$.) After n steps the concentration is $C = 2^{-n}(C_0 - C_P) + C_P$, and because $C_P \ll C_0$, $C = 2^{-n}C_0 + C_P = C_n + C_P$, where $C_n = 2^{-n}C_0$ is the nominal concentration. At each step we measured the attachment frequency ν_A at constant temperature and pressure ($T = 77.4$ K, $P = 21$ atm). The results are plotted in figure 3 against C_n. The dependence is linear as expected. The intercept at $\nu_A = 0$ yields $(-C_P)$. For our partially purified helium, C_P results to be $C_P \simeq 10^{-7}$. If we calculate the rate coefficient $K = (\nu_A / N_{He} N_{O_2})$ we get 6.0×10^{-34} cm^6 s^{-1}, to be compared with $K = 6.1 \times 10^{-34}$ cm^6 s^{-1} found at the same temperature and pressure by Bartels (1974).

3.2. Attachment peak

Several measurements of attachment frequency have been made, varying the helium density in the range $(1\text{–}5) \times 10^{21}$ cm^{-3}. The lower limit in N was fixed by the density at which the β particles reach the first grid G_1, and the higher limit was given by the maximum pressure available in the cell. The maximum attachment occurs at a density $N_P \simeq 3 \times 10^{21}$ cm^{-3}, nearly one-third of the helium critical density. At $N = N_P$ the mean interatomic separation is $(N_P)^{-1/3} \simeq 7$ Å, while the mean free path for the injected electrons would be $(\sigma N)^{-1} \simeq 80$ Å. This last value has not much sense, obviously, because the spatial extent of the electron wave packet is of the order of $\hbar(3/2mE)^{1/2} \simeq 11$ Å for $E = 0.091$ eV. The above figures are anyhow useful to enlighten the physical situation of the experiment.

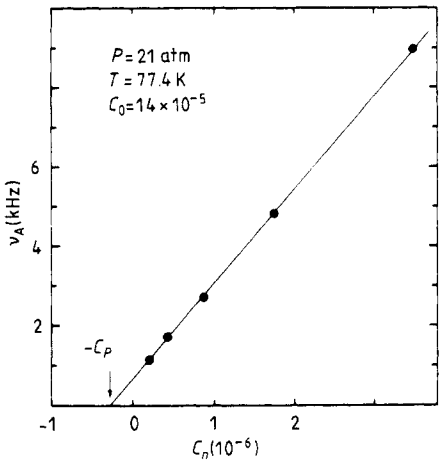

Figure 3. Attachment frequency ν_A plotted against nominal O_2 concentration C_n. C_0 is the O_2 concentrations at the beginning of the dilution procedure. C_P is the O_2 concentration of the 'pure helium'.

The measurement of ν_A involves the ratio between the total current $(I_0/2)$ and the electronic current I^*. The best situation for the measurement is to have an electronic current of the same order as the ionic one. If the attachment is too strong or too weak the errors become too great. The oxygen concentration was therefore adjusted run by run to have $I^* \simeq \frac{1}{2}(I_0/2)$. In this situation $\nu_A \simeq 2f_e \ln 2$. Using typical values, $E = 50\ \mathrm{V\,cm^{-1}}$, $d = 0.5\ \mathrm{cm}$, $\mu_e \simeq 60\ \mathrm{cm^2\,V^{-1}\,s^{-1}}$ at $N = N_P$, we have $v_D \simeq 3 \times 10^3\ \mathrm{cm\,s^{-1}}$, $f_e = 1/2\tau_e \simeq 3 \times 10^3\ \mathrm{Hz}$, and finally $\nu_A \simeq 4100\ \mathrm{Hz}$. Actually the mean value of ν_{AP} at the peak density N_P for all our runs was 5700 Hz. We can use Bartels data to estimate the oxygen concentration to be used in the best conditions. At 77 K he found for the maximum attachment $\nu_{AP} = (2.6 \times 10^{11}\, C)$ Hz, where C is the oxygen concentration. For $\nu_{AP} \simeq 4100$ Hz the concentration must therefore be $C \simeq 2 \times 10^{-8}$.

At this low level it was not possible to use a pre-fixed and measured impurity content. We worked therefore in each run with helium gas of unknown but constant impurity concentration. The measurements were taken both increasing and decreasing the pressure in the cell, in order to check on systematic errors due to possible change in C during the run. To test the correct operating of our injection and measuring technique, we measured ν_A, at a fixed temperature and density, for different values of the electric field applied to the drift space, in the range $10 < E < 100\ \mathrm{V\,cm^{-1}}$. While the cut-off frequency f_e ranged from 0.8 to 25 kHz, the attachment frequency calculated through relation (10) turned out to be independent of E, as expected.

As will be shown in § 4 the ratio (ν_A/N^2) should be proportional to $F(E_R, N)$, the value of the energy distribution function at $E = E_R$. The multiplicative constant, however, is not known because we know neither the impurity concentration C, nor the stabilising probability p_s. The data for the ratio (ν_A/N^2) are therefore reported as reduced data $\nu^* = (\nu_A/N^2)/(\nu_A/N^2)_{max}$ normalised to unity at their maximum value. The results obtained at $T = 51.0$, 64.9, 77.4 and 89.3 K, are plotted in figure 4 and they should be representative of the normalised energy distribution function $F_N(E_R, N)$ at $E = E_R$. The dependence on density is faster at the low density side of the peak than at the other one. Except the data very near to the maximum, the experimental points can be well fitted by exponential functions, $\nu^* = \exp[-b_1(N_1 - N)]$, low side,

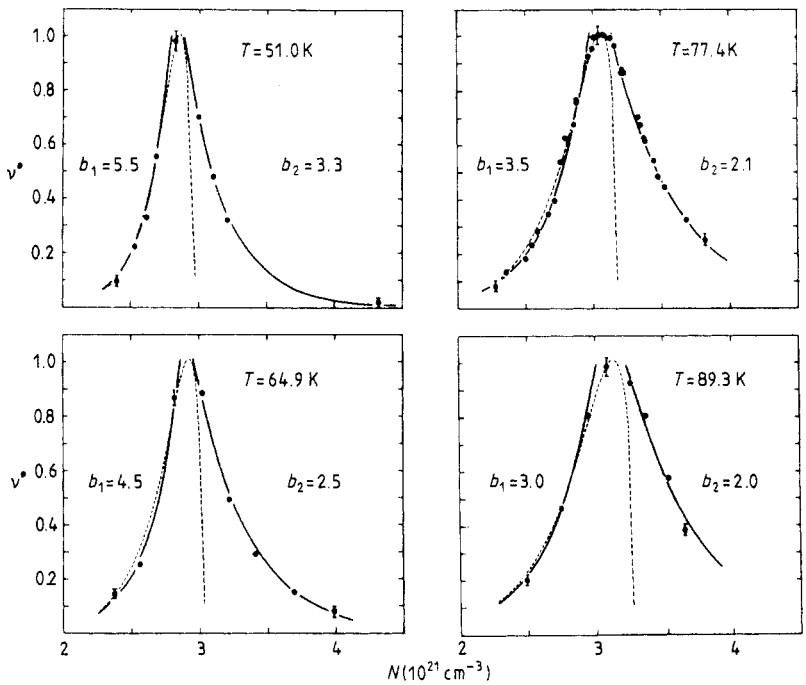

Figure 4. Reduced attachment coefficient ν^* plotted against helium number density at four different temperatures. The broken curves represent the classical shifted distribution (17), and the full curves are the fitting functions explained in the text. The values of parameters b_1 and b_2 are expressed in 10^{-21} cm^3.

and $\nu^* = \exp[-b_2(N-N_2)]$, high side. The parameters b_1 and b_2 are temperature dependent and are quoted in figure 4.

The peak reaches its maximum at a density N_P, which is between N_1 and N_2. The density value N_P of the maximum attachment, defined as $N_P = (N_1+N_2)/2$, is shown in figure 5. The peak density N_P increases slightly with temperature, as $N_P = (2.36+8.8\times10^{-3}\,T)\times10^{21}\,\text{cm}^{-3}$. This result is unexpected, because when we have a greater thermal contribution to the electron energy, we expect that a smaller density shift contribution would be needed to reach the resonant energy. Therefore N_P should decrease with temperature, quite the opposite of the behaviour found in the experiments. It is hard to see how more refined calculations could give an inverted temperature dependence, if no other effects are introduced.

The resonant density N_R calculated through relation (2) with $a = 0.62$ Å, would be $N_F = 30.6\times10^{20}\,\text{cm}^{-3}$, about the value of N_P at 77 K. We work however at rather high densities where the low density approximation given by the relation (2) is no more valid. If we use the well known Wigner–Seitz model (Wigner and Seitz 1933, Eggarter 1972), we get $N_{WS} = 2.37\times10^{21}\,\text{cm}^{-3}$, figure 6. This is the same value one obtains extrapolating the experimental results to zero temperature (figure 5). Because at $T = 0$ K there is no thermal contribution to the energy, this value of N_R is the local density sensed by the electron at resonance. At the temperatures of our experiments, one needs a mean density N greater than N_R to bring the extra electron to the resonant energy E_R. This suggests the local density N' around the electron to be smaller than N, as a result of the electron–medium interaction, and this effect should be linearly dependent on temperature. An alternative explanation can be found supposing the

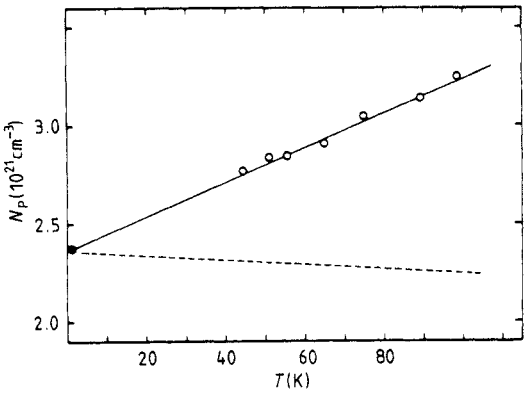

Figure 5. The measured peak density N_P (open circles) plotted against temperature T. The straight line is the best fit of the data reported in the text. The full circle at $T \simeq 0$ is the value of the resonance density N_R as calculated by the Wigner–Seitz model. The broken curve represents relation (18).

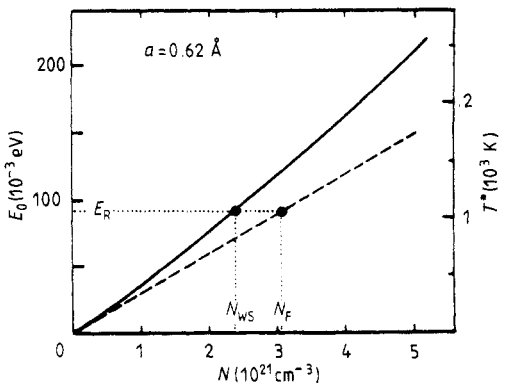

Figure 6. The electron self-energy E_0 plotted against scatterers number density N calculated for $a = 0.62$ Å. Full curve: from the model of Wigner and Seitz (1933). Broken curve: from the Fermi theory (1934).

energy E_R to be affected by the presence of the high-density helium gas, which can change the vibrational energy levels of both ion and neutral oxygen molecule.

The local density depletion, and a possible dependence of E_R on the local density, raise some problems about the idea that the electron energies can be accurately sampled by molecular impurities. We observe, however, that these effects are not very great. N_P in fact changes about 18%, changing the temperature from 50 to 100 K. We hope that these minor problems can be solved when more data will be available at lower and higher temperatures, on different gases and with different impurities.

The width of the peak at half height is plotted in figure 7 as a function of temperature. It comes out to be proportional to the absolute temperature T, $\Delta N = (8.8 \times 10^{18}\, T)\,\mathrm{cm}^{-3}$. Converting ΔN to energy by the relation $\Delta E = b\,\Delta N$, we find that the peak has an energy spread at half height $\Delta E = 4.0\, k_B T$, if we use for b the value given by the Wigner–Seitz model at the density $N = 3 \times 10^{21}\,\mathrm{cm}^{-3}$, $b = 6.3 \times 10^{-35}\,\mathrm{erg\,cm}^3$. We must point out now that the spin coupling in the $X\,^2\Pi_g$ state of the O_2^{-*} splits each level into a doublet. For $n = 4$ it leads to $E_4(\Pi_{1/2}) = 0.081$ eV and $E_4(\Pi_{3/2}) = 0.100$ eV (Land and Raith 1973). The 20 meV separation between the

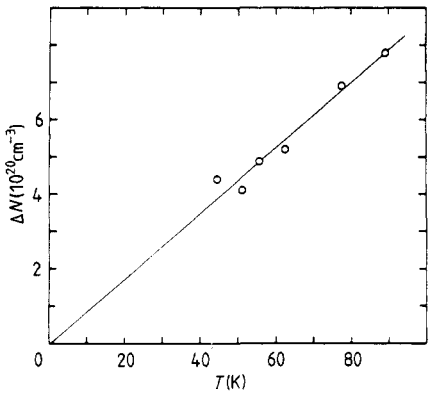

Figure 7. The measured peak width ΔN at half height, plotted against temperature T. The full curve is the linear best fit reported in the text.

doublet components would correspond to a density difference $\Delta N_d \simeq 5\times10^{20}\,\mathrm{cm}^{-3}$. The measured attachment peak does not show however any doublet structure, even at the lowest explored temperature (figure 10), where the peak width is less than ΔN_d. One might suppose the doublet pattern to be smoothed out by the line broadening due to the electron energy distribution function or to density fluctuations (Bartels 1974, Jahnke *et al* 1975). But this argument could only work for the high temperature results where $\Delta N > \Delta N_d$, and it fails at $T \leqslant 60\,\mathrm{K}$ where $\Delta N \leqslant \Delta N_d$. We have no explanation for the absence of the doublet pattern. As this detail is not clear, we use in the following the mean value $E_R = 0.091$ eV.

4. Discussion

4.1. Collisions and capture

Let n, N and N_2 be the number of extra electrons, helium atoms and oxygen molecules per unit volume. The number dn of electrons that are captured by an oxygen molecule in a time interval dt is given by $dn_1 = dt\, nN_2 \int_0^\infty \sigma(E)v(E)F(E,N)\,dE$, where $\sigma(E)$ and $v(E)$ are the capture cross section and electron velocity at the energy E, and $F(E,N)$ is the electron energy distribution function at the helium density N.

The capture cross section has its maximum at $E = E_R$. Its width $\Delta E \simeq \hbar/\tau$ should be about 3×10^{-4} eV if we assume a mean life $\tau \simeq 2\times10^{-12}$ s as suggested by experiments in high-density nitrogen gas (Christophorou 1978). The width of $F(E)$ is about $4\,k_B T$, that is $\Delta E' \simeq 1.7\times10^{-2}$ eV at $T = 50$ K. Both $F(E,N)$ and $v(E)$ are slow-varying functions with respect to $\sigma(E)$, and therefore

$$dn_1 = dt\, nN_2 v(E_R)F(E_R,N)\sigma_c \tag{14}$$

where $\sigma_c = \int_0^\infty \sigma(E)\,dE$ is the capture integrated cross section, and $v(E_R) \simeq 1.8\times10^7\,\mathrm{cm\,s}^{-1}$. At our drift velocities, $v_D \simeq (10^3\text{–}10^4)\,\mathrm{cm\,s}^{-1}$, we also found that both (v_D/E) and the attachment frequency ν_A do not depend on the electric field. Therefore the electric fields used in our experiments, $E \simeq 50\,\mathrm{V\,cm}^{-1}$, should not affect the equilibrium distribution function. The removal of electrons at $E = E_R$ is a negligible effect. In fact because $N_2 \simeq 3\times10^{-8}\,N$, in a mean electron–oxygen collision time the electron can be thermalised by many collisions with helium atoms. We can assume, to conclude, that $F(E,N)$ is the equilibrium distribution function.

The oxygen molecule number density N_2 is also practically unaffected by the attachment process. Using typical values $j = 10^{-11}$ A cm^{-2}, and $v_D = 5 \times 10^3$ cm s^{-1}, we get $n = 1 \times 10^4$ cm^{-3} for the electron density, while $N_2 \simeq 10^{14}$ cm^{-3}. The removal of oxygen molecules by the electron beam is therefore a negligible effect.

Only a fraction p_s of the dn_1 excited ions are stabilised into the ground state. The electron number density will change as $dn = -p_s\, dn_1 = -n\nu_A\, dt$. By integration we get the exponential decay of § 2.1, $n(t) = n(0) \exp(-\nu_A t)$, where

$$\nu_A = \sigma_A N_2 v(E_R) F(E_R, N) \tag{15}$$

where $\sigma_A = (p_s \sigma_c)$ is the effective integrated attachment cross section.

If the attachment is a two-stage process, then dn_2 out of the dn_1 temporary ions dissociate by spontaneous decay into a free electron and a neutral molecule, dn_3 are stabilised into the ground state by a helium atom collision, and dn_4 are dissociated by an analogous collision. It can be shown that at our electron, oxygen and helium densities, the ratio between the rates of removal and production is very high. More precisely, each excited ion can decay long before another one is created in the drift volume. There is no accumulation of excited ions in the drift volume, we have only free electrons and stabilised ions. For such a situation the fraction p_s is simply $p_s = (K_3 N)[K_2 + N(K_3 + K_4)]^{-1}$ where $K_2 = \tau_0^{-1}$, τ_0 being the autoionisation lifetime, and K_3 and K_4 are the rates for collisional stabilisation and dissociation, respectively. If we use the accepted value of $\tau_0 = 2 \times 10^{-12}$ s and the Langevin–Wannier H_e–O_2^- cross section (Goans 1974), then $K_2 = 5 \times 10^{11}$ s^{-1}, and $N(K_3 + K_4) = 34 \times 10^{11}$ s^{-1} at $N = 3 \times 10^{21}$ cm^{-3}. The stabilisation probability p_s should therefore be almost density independent.

Our knowledge on the attachment process in low-density gas cannot be so simply translated at high densities, where the simple Bloch–Bradbury mechanism breaks down (Christophorou 1978). Both the integrated capture cross section σ_c and the stabilisation probability p_s may depend on density, and from the measurement of ν_A we can only infer the density dependence of $\sigma_A = (p_s \sigma_c)$, which can be calculated by (15) if we know the density dependence of the distribution function.

4.2. The classical shifted distribution

The calculation of the distribution function for our system is a very difficult and unsolved problem, in that we are dealing with a highly disordered system. The extra electrons in fact sense the helium density in a rather small volume, and the self-energy fluctuates around a mean value because of the density fluctuations.

It is useful as a first point to consider briefly a simple model that completely neglects the density fluctuations. It is an unrealistic model, but it can help the discussion of the experimental data. In this model the self-energy E_0 is the same for each electron, and the density of states is given by the well known relation $g_0(E) = A(E - E_0)^{1/2}$, where $A = (V/2\pi^2)(2m/\hbar^2)^{3/2}$. We expect that the real $g(E)$ has a tail around the edge at $E = E_0$, because of the self-energy fluctuation ΔE_0. At an energy E_R such that $\Delta E_0 \ll (E_R - E_0)$, however, $g(E)$ should not be very different from $g_0(E_R)$. The partition function $Z(N)$ and the distribution function $F(E, E_0)$ are therefore

$$\begin{aligned} Z(N) &= (2V/\hbar^3)(2\pi m k_B T)^{3/2} \exp(-E_0/k_B T) \\ F(E, E_0) &= D(E - E_0)^{1/2} \exp[-(E - E_0)/k_B T] \end{aligned} \tag{16}$$

where $D=(2/\pi^{1/2})(k_BT)^{-3/2}$. The effect of the uniform self-energy E_0 is simply to translate the classical distribution by an amount $E_0=bN$. Changing the helium density we change the shift, while the attachment process samples the energy distribution at the fixed energy $E=E_R$ (figure 8). The density dependence at $E=E_R$ will be

$$F(E_R, N)=D(E_R-bN)^{1/2}\exp[-(E_R-bN)/k_BT]. \tag{17}$$

The maximum has the value $F_M=(3.5\times10^{15}/T)\ \mathrm{erg}^{-1}$, which does not depend on the values of b and E_R, and it is attained at the density

$$N_M=(E_R-\tfrac{1}{2}k_BT)/b. \tag{18}$$

The width at half height is $\Delta N=(1.8\ k_BT/b)$.

The relation (17) should be the correct energy distribution function to be used in relation (15) at $N<N_P$. We may use the relations (15), (17), together with the measured ν_A, to calculate $\sigma_A(N)$. At 77.4 K we find that in the density range

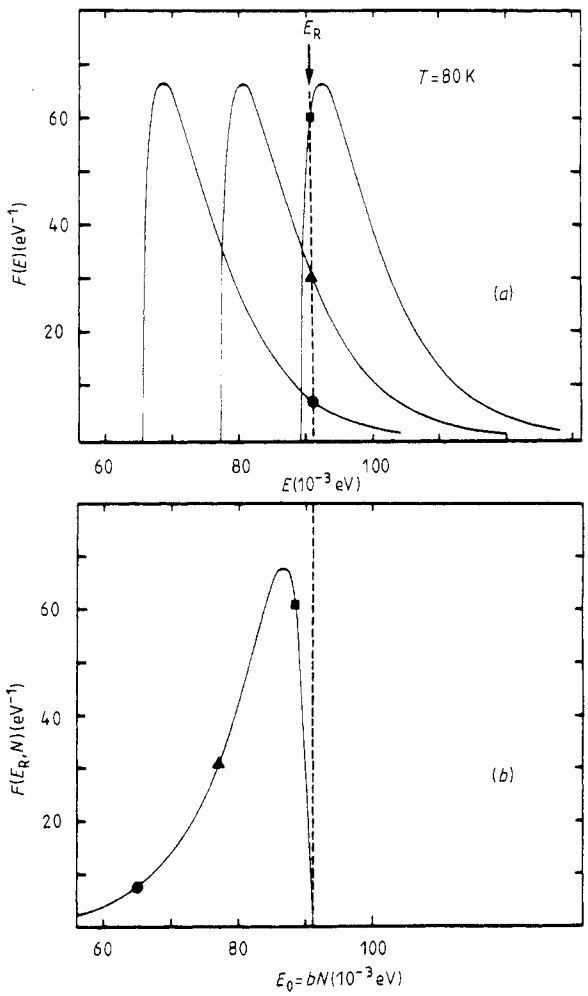

Figure 8. (*a*) The classical shifted energy distribution function $F(E, N)$ drawn for $N=22$, 26 and 30 ($\times10^{20}\ \mathrm{cm}^{-3}$). (*b*) The same distribution calculated at $E=E_R$ as a function of the shift $E_0=bN$.

$(19\text{–}30)\times10^{20}$ cm^{-3} (σ_A/N) is density independent within experimental errors. Using moreover our data at known oxygen concentration and those reported by Bartels (1974), we get $\sigma_A \simeq 2\times10^{-41}N$ (eV cm^2). We do not know exactly whether the integrated capture cross section σ_c is constant or density dependent. If we assume for σ_c a constant value $\sigma_c = 5\times10^{-19}$ eV cm^2, as calculated theoretically (Parlant and Fiquet-Fayard 1976), we get $p_s = (\sigma_A/\sigma_c) \simeq 4\times10^{-23}N$, that is $p_s \simeq 0.12$ at $N = 30\times10^{20}$ cm^{-3}.

This point must certainly be investigated more carefully at lower densities, but we observe that it is not so important to know the exact density dependence of σ_A, because $F(E_R, N)$ depends strongly on N, and because the resonance peak covers a restricted density range. Taking the above results as a suggestion we assume as a reasonable approximation $(p_s\sigma_c) = \sigma^*N$ in the whole density range investigated. Because ν_A has been measured at constant oxygen concentration, then $N_2 = CN$ and so (ν_A/N^2) can be taken as proportional to $F(E_R, N)$.

The function $F(E_R, N)$, normalised to unity at its maximum, as $F_N = F(E_R, N)/F_M$, is plotted in figure 4 where b was chosen to give the best fit of the data at each temperature. The values of b decrease with temperature and are shown in figure 9. The dependence of b on temperature is not understood, being the same problem as the unexpected temperature dependence of the peak density N_P (§ 3.2).

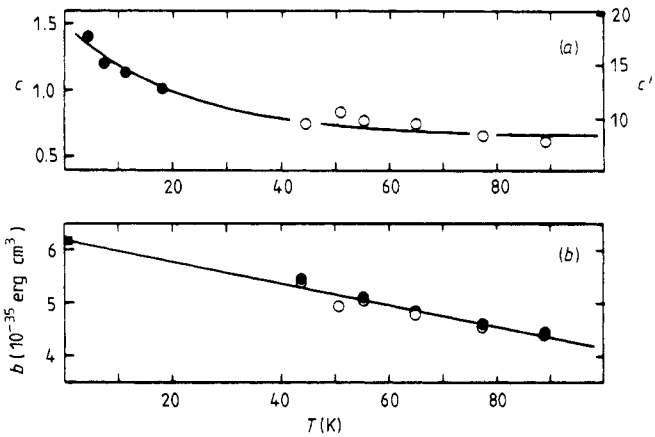

Figure 9. The values of coefficients c and b (open circles) used to fit the peak shape with the model of Eggarter and Cohen. (*a*) The full circles are the values used in the fit of mobility data (Eggarter 1972). The full curve is the interpolating function given in the text. (*b*) Full circles are the values used with the classical shifted distribution. The square at $T \simeq 0$ is the value given by the Wigner–Seitz model. The full curve is the best fit given in the text.

At a given temperature, the function (17) describes well the data up to the maximum of the peak, where it falls rapidly to zero because it neglects the density fluctuations. The high-density side of the peak is therefore representative of the tail states, that can be detected in a rather direct way by the attachment experiments.

4.3. A semiclassical model

We try to take into account the density fluctuations using the semiclassical model of Eggarter and Cohen (1970). The probability $dP = P(N')\,dN'$ of finding the density between N' and $N' + dN'$ inside a small volume V_F in the gas of a mean density N,

is given by the Gaussian distribution $P(N') = (2\pi\sigma_N^2)^{-1/2} \exp[-(N'-N)^2/2\sigma_N^2]$ where $\sigma_N^2 = (N^2 k_B T k / V_F)$. At our temperatures we can use for k the isothermal compressibility of the ideal gas, $k = (1/Nk_BT)$, and with the position $V_F = L^3$ we have

$$P(N') = 0.4(L^3/N)^{1/2} \exp[-0.5(L^3/N)(N'-N)^2]. \tag{19}$$

In the model of Eggarter and Cohen the macroscopic volume V is divided into W equal cells of volume $L^3 = (V/W)$. The number of cells dW with a density between N' and $N' + dN'$, is given by $dW = WP(N')\,dN'$, where $P(N')$ is given by (19). There are two strong assumptions in the model.

(i) The volume L^3 over which the density is averaged to construct the Wigner–Seitz potential is assumed to be of the order of $(\Delta x)^3$, Δx being the spatial extent of the electron wave packet.

(ii) The density of states for each cell has the same form as that of a particle in a macroscopic box of side L, shifted along the energy axis by an amount bN', $g'(E) = A'L^3(E - bN')^{1/2}$, where $A' = (1/2\pi^2)(2m/\hbar^2)^{3/2}$. The contribution to the density of states given by the dW cells with the same N', is $dG = g'(E)\,dE\,WP(N')\,dN'$. Summing all the contributions at various densities, we have

$$g(E, N) = A \int_0^{N_E} (E - bN')^{1/2} \exp[-0.5(L^3/N)(N'-N)^2]\,dN' \tag{20}$$

where $A = 0.4V(L^3/N)^{1/2}A'$, $N_E = E/b$.

Our measurements run over a restricted density range, and as a first approximation we can assume L to be density independent. The widths of our experimental peaks are reproduced by this model with a choice of $L \simeq 45$ Å. A cell of this size contains about 270 atoms at $N = 3 \times 10^{21}$ cm^{-3}.

As a next approximation we assume that $L = c\Delta x$ where c is a constant and Δx is the spatial extent of the electron wave packet. The shape of the attachment peak obtained in this way is not much different from that obtained with the use of a constant L, but it is useful to proceed in this way to compare our analysis with that of mobility data. Following, therefore, Eggarter and Cohen we assume $L = ch(3/2mE')^{1/2}$, where c is a constant to be determined by the fit of the experimental data, and E' is a representative value for the energies at the mean density N, $E' = bN$. With this position $L = ch(3/2mbN)^{1/2}$, and

$$g(E, N) = A \int_0^{N_E} (E - bN')^{1/2} \exp[-B(N'-N)^2]\,dN' \tag{21}$$

where

$$A = 19.3\ V(c/h^3)(m/b)^{3/4}N^{-5/4}$$

$$B = 0.5\ h^3(3/2m)^{3/2}(c^3/b^{3/2}N^{5/2}).$$

Once some values for b, c, N and T have been fixed, $g(E, N)$ and the partition function $Z(N, T)$ can be computed by numerical integration.

The energy distribution function for $E = E_R$ is then $F(E_R, N) = [g(E_R, N)/Z(N)] \exp(-E_R/k_BT)$, and finally the reduced energy distribution function is $F_N = F(E_R, N)/F_{max}$, normalised to unity at its maximum. The constants b and c are chosen to get the best position of the peak at the lower density side, as in § 4.2, and the correct width of the peak at half height. The fit is very sensitive to the choice of the parameters. We used a fixed value of $E_R = 0.091$ eV as in § 4.2. The values of

the parameters b and c are shown in figure 9, together with the values of b used in the classical distribution without fluctuations.

The values of parameter b can be fitted by the linear relation $b = (6.17 - 2.1 \times 10^{-2}\, T) \times 10^{-35}$ erg cm^3, indicating that the Wigner–Seitz value b_{WS} is approached at zero temperature. This problem is of course the same as the temperature dependence of the peak density discussed in § 4.2. The values obtained for the parameter c are shown also in figure 9, together with those obtained in the analysis of the mobility data (Eggarter 1972). Both groups of data can be fitted by the function $c = 0.65 + 0.83 \exp(-4.5 \times 10^{-2}\, T)$. All the values are situated along a unique curve, despite the different nature of the two experiments, and this is undoubtedly an

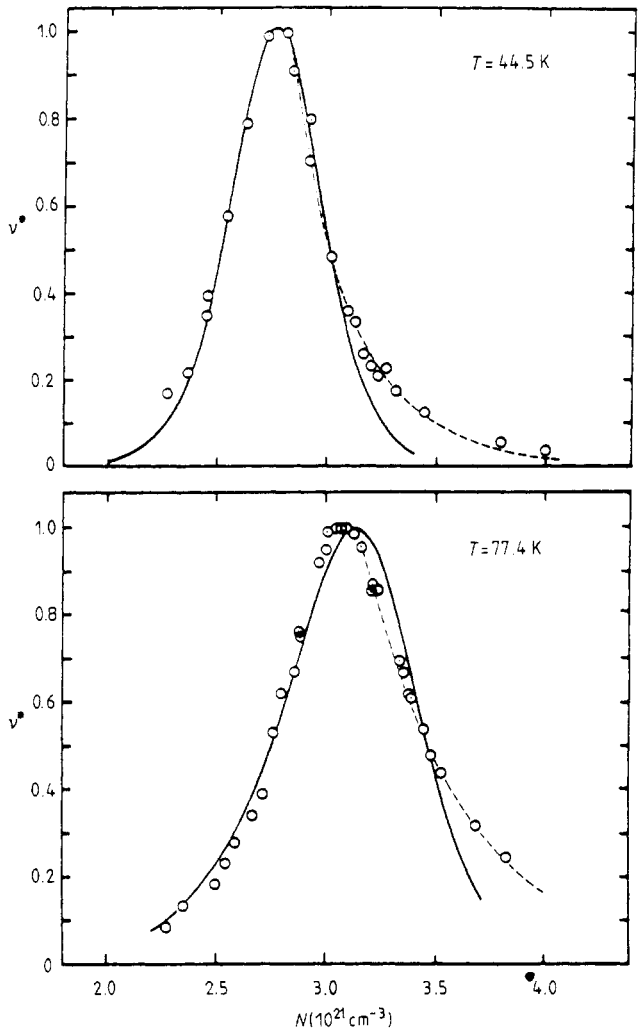

Figure 10. The reduced attachment frequency ν^* plotted against helium number density N at $T = 44.5$ K and $T = 77.4$ K. The full curves represent the density dependence of the reduced energy distribution function as calculated through the model of Eggarter and Cohen. The broken curves are the fitting functions of § 3.2. The b and c values used in this calculation are those of figure 9.

encouraging result, even if one can not attribute a particular physical meaning to the interpolating function. For temperatures greater than about 20 K, the constant c is smaller than unity, indicating that the electron samples the density in a volume V_F smaller than the spatial extent of the wave packet; that would be an absurd result. The constant $c=(L/\Delta x)$ has been introduced using firstly the relation $\Delta p\,\Delta x=\hbar$ (Eggarter and Cohen 1970), and later $\Delta p\,\Delta x=\hbar$ (Eggarter and Cohen 1971, Eggarter 1972). If we use the more correct expression $\Delta p\,\Delta x\geqslant\hbar/2$, assuming $L=c'(\hbar/2)/\Delta p$, we get a new constant $c'=4\pi c$, and even at high temperature we have $L\simeq 8\,\Delta x$, a result that does not violate the uncertainty principle.

The behaviour of the computed F_N is shown in figure 10 for two different temperatures. F_N fits the data at the lower density side of the peak rather well, but it falls faster at the higher side. This result should not be a surprise, since the model assumes the states in a cell of side $L\simeq 45$ Å to be continuously distributed in the same way as for a macroscopic cell. This can be a reasonable approximation at the lower density side of the peak, where the resonant attachment samples on the upper side of the density distribution (figure 11). The cells have there a density N' greater than the mean density N, and they should therefore be mainly surrounded by cells with lower densities, which means by regions with lower potentials. The states are essentially extended, and the assumed density of states can be a good approximation, as already shown in § 4.2 by using the oversimplified model that completely neglects the density

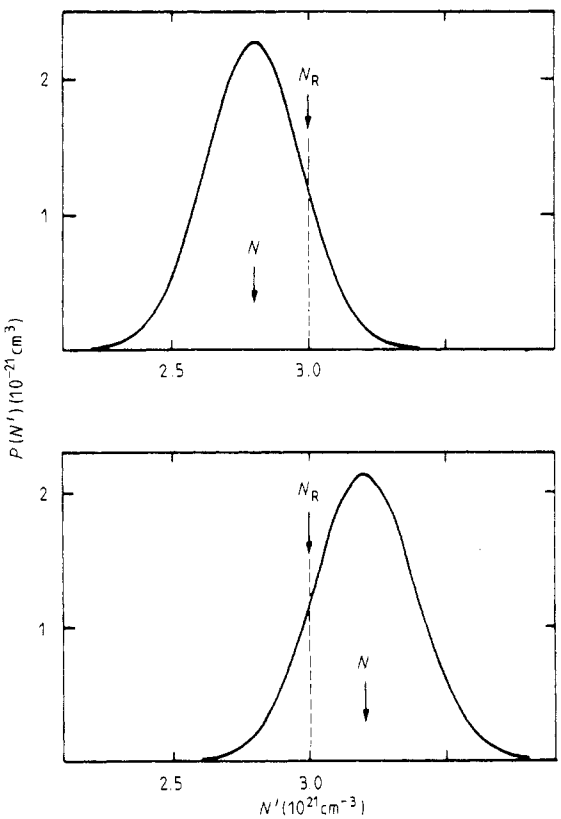

Figure 11. The Gaussian distribution of the local density N' calculated for a mean density N lower and higher than the resonance density N_R, and for a cell side $L=45$ Å.

fluctuations. The opposite occurs at the higher density side of the peak, where cells with $N' < N$ are sampled by the oxygen molecules. In this case the states should be localised over small regions and the use of the quasi-continuous density of states of a macroscopic box becomes a rough approximation.

5. Conclusions

The analysis of the attachment process in dense helium gas revealed a number of features and problems that must be further investigated, both theoretically and experimentally. Among them the absence of a doublet structure in the attachment peak, and an unexpected temperature dependence of the position of maximum attachment, which is probably due to a local density effect. The density dependence of the effective attachment cross section must be investigated at higher oxygen concentration and at lower helium densities, where a reasonable 'classical' energy distribution function can be used. Nevertheless, because the resonance peak covers a restricted density range, it is possible to connect with enough confidence the attachment frequency to the energy distribution function. The experimental method gives useful and unique information on the energies near the mobility edge, where density fluctuations are important. The detailed analysis of the experimental results is not simple, however. The mean helium density needed to bring extra electrons into resonance with the oxygen molecules gives results higher than that predicted by the Wigner–Seitz model. This suggests that the local density around the extra electron should be smaller than the mean density, an effect gradually disappearing at $T \to 0$. While the semiclassical model of Eggarter and Cohen explains quite well the giant decrease in the electron mobility as the helium density is increased, it is inadequate to describe the shape of the attachment peak, even if from the width of the peak one obtains a size of sampling cell that is consistent with that obtained by mobility data.

Our problem is related to the calculation of the electronic energy distribution in a disordered system, a very general and difficult problem. A great amount of theoretical work has been performed in this field, but many problems remain still open. The results of the present experiment indicate that the resonant attachment can be an important test for the theories and a means for a deeper understanding of the disordered systems.

References

Bartels A K 1973 *Phys. Lett.* **45A** 491
—— 1974 *Thesis* University of Hamburg
Boness M J W and Schulz G J 1970 *Phys. Rev.* A **2** 2182
Bruschi L, Santini M and Torzo G 1983 to be published
Burdick B 1965 *Phys. Rev. Lett.* **14** 11
Christophorou L G 1971 *Atomic and Molecular Radiation Physics* (London: Wiley Interscience)
—— 1978 *Adv. Electron. Electron Phys.* **46** 55
Cook G A 1961 *Argon, Helium and the Rare Gases* (New York: Interscience)
Cunsolo S 1961 *Nuovo Cimento* **21** 2644
Eggarter T P 1972 *Phys. Rev.* A **5** 2496
Eggarter T P and Cohen M H 1970 *Phys. Rev. Lett.* **25** 807
—— 1971 *Phys. Rev. Lett.* **27** 129
Fermi E 1934 *Nuovo Cimento* **11** 157

Goans R E 1974 *Thesis* University of Tennessee
Hatano Y and Shimamori H 1981 *Electron and Ion Swarms* ed L G Christophorou (New York: Pergamon)
Herzenberg A 1969 *J. Chem. Phys.* **11** 4942
Jahnke J A, Silver M and Hernandez J P 1975 *Phys. Rev.* B **12** 3420
Jortner I, Kestner R N, Rice S A and Cohen M H 1965 *J. Chem. Phys.* **43** 614
Land J F and Raith W 1973 *Phys. Rev. Lett.* **30** 193
Northby J A and Sanders T M 1967 *Phys. Rev. Lett.* **18** 1189
Parlant G and Fiquet-Fayard F 1976 *J. Phys. B: At. Mol. Phys.* **9** 1617
Schoepe W and Rayfield G W 1973 *Phys. Rev.* A **7** 2111
Sommer W T 1964 *Phys. Rev. Lett.* **12** 271
Tauchert W J, Jungblut H and Schmidt W F 1977 *Can. J. Chem.* **55** 1860
Wigner E and Seitz F 1933 *Phys. Rev.* **43** 804
Woolf M A and Rayfield G W 1965 *Phys. Rev. Lett.* **15** 235